Design and Full Characterization of a 3-D-Printed Hyperbolic Pyramidal Wideband Microwave Absorber

Xhoandri Lleshi, Thi Quynh van Hoang, Brigitte Loiseaux, Didier Lippens

Design and Full Characterization of a 3D-Printed Hyperbolic Pyramidal Wideband Microwave Absorber

Xhoandri Lleshi, Thi Quynh Van Hoang, Brigitte Loiseaux and Didier Lippens

***Abstract*—A fully 3D printed wideband metamaterial absorber, characterized by an absorptivity above 0.95 in the X and Ku bands and with a fractional bandwidth of 0.71, is presented in this paper. A 250 mm x 250 mm sample, with a total thickness of 6.3 mm ($0.26\lambda_0$), is fabricated exploiting the fused deposition modeling technique with commercial filaments. To achieve a wideband absorption, a hyperbolic metamaterial with a pyramidal shape is designed by vertically stacking multiple resonant cavities. Lossy filaments are used to increase the dissipative losses and cavities with tailored dimensions are designed to absorb equidistant frequencies to obtain a unitary and flat absorption. The measurements are performed for different azimuth and incident angles, for both vertical and horizontal polarizations in anechoic and non-anechoic chambers. For normal incidence, thanks to the symmetry of the structure, quasi-unitary absorption is obtained over a wide frequency range from 8.2 GHz to 17.2 GHz for azimuthal rotations of 90°. For oblique incidence, the absorption behavior in vertical polarization is better than the one in horizontal polarization. Two cases at azimuth angles of 0° and 30°, corresponding to the best and the worst performances of the presented absorber, are here presented.**

***Index Terms*—fused deposition modeling, hyperbolic metamaterial, radar absorbing material, wideband absorber**

I. Introduction

MICROWAVE absorbers have been used in various domains such as stealth technology, EM compatibility, anechoic chamber, etc. The first absorbers were developed during the WWII with a resonant behaviour. The Salisbury screen [1],[2] and the Jauman screen [3] are based on resistive losses to dissipate the energy. The same concept with dielectric losses is exploited in the Dallenbach screen [4]. The main problem of these structures is the total thickness, considered too thick for many practical applications, since it is directly linked to quarters of the absorbed wavelengths [5]. In 2002, a solution was suggested by Engheta with a resistive layer posed on a metamaterial surface working as HIS (High Impedance Surface), spaced from a reflective plate a distance much smaller than λ/4 [6].

This work has been partly funded by the French MOD.

X. Lleshi, T. Q. V. Hoang and B. Loiseaux are with Thales Research and Technology, 91120, Palaiseau, France (xhoandri.lleshi@thalesgroup.com, van.hoang@thalesgroup.com, brigitte.loiseaux@thalesgroup.com).

D. Lippens is with IEMN, Villeneuve-d'Ascq, 59650, France (didier.lippens@univ-lille.fr).

So far, many metamaterial and metasurface absorbers have been developed [7]-[14]. In 2008, the first perfect metamaterial absorber was fabricated by Landy et al. with unitary absorption at 11.65 GHz [15]. Another phenomenon for narrowband absorption is obtained with metal-insulator-metal (MIM) cavities which permit to match the free space impedance, assure no transmission and confine the field inside the lossy dielectric layer [16]. To enhance the bandwidth of MIM structures, two approaches are followed. The first one is to employ a superposition of cavities with different widths corresponding to the superposition of multiple absorbed frequency peaks, the so-called hyperbolic metamaterials (HMM) [17]. The second is related to the losses on the conductive layers as well as on the dielectric layers [18]. It is well known that a cavity can be characterized by its quality factor; a low quality factor permits to enlarge the bandwidth with a meaningless reduction of the absorption level [19].

The HMM notion was firstly introduced in optics [20]. In 2012, this concept was brought by Ding et al. to RF domain with a pyramidal shape HMM made of 20 pairs of layers, fabricated using the PCB technology, with an absorptivity of 0.9 over the frequency range of 7.8–14.7 GHz [21]. This concept offers numerous interesting characteristics required nowadays to the radar absorbing materials (RAMs) such as broadband absorption [22], high robustness in incidence angles [23] and low profile, which is less than 1 cm for Ding's structure. The limitation of the absorber presented in Ding's work is the use of PCB technology. The main drawbacks of this technology are the impossibility to work toward the vertical axis, for instance changing the thickness of some desired cavities, the difficulty to fabricate a stair-like shape with the desired widths, and the limitation on working only with planar surfaces. These weaknesses can be overcome with the 3D printing technology. Since the first patent on 3D printed absorber in 2016 [24], many studies on RAM using this new technology were conducted by exploiting arbitrary geometries as well as tailor-made materials [25]-[32].

In this paper, the hyperbolic pyramidal concept is harnessed and extended with the introduction of the losses of the conductive filament to increase the dissipated power and decrease the quality factor, presenting a first RAM prototype fully fabricated in Fused Deposition Modeling (FDM) technology able to absorb a wideband frequency (X, K_u-bands) with only 10 pairs of layers.

II. Unit Cell Design

When a surface is impinged by a wave, the energy must be reflected, transmitted or absorbed following the energy conservation law as described by (1):

$$1 = A(f) + \left|S_{11}(f)\right|^2 + \left|S_{21}(f)\right|^2 \quad (1)$$

where $A(f)$ is the absorptivity, $|S_{11}(f)|^2$ is the reflectivity, $|S_{21}(f)|^2$ is the transmissivity and f is the frequency. In order to achieve unitary absorption A(f) = 1, $S_{11}(f) = 0$ and $S_{21}(f) = 0$ need to be satisfied. In our design, zero transmission is obtained by placing a metal plate on the bottom of the structure while zero reflection is achieved with the impedance matching that is accomplished when a cavity resonates.

The unit cell is composed by stacking 10 pairs of dielectric and conductive square layers on a ground plane as shown in Fig. 1 [30].

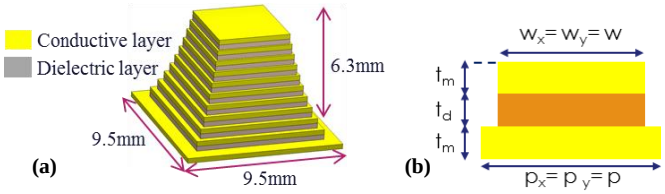

Fig. 1: (a) Unit cell design with the pyramidal shape, (b) single MIM (Metal-Insulator-Metal) cavity.

The single cavity is completely defined by four parameters, as shown in Fig. 1(b): the width w of the top layer, the period p of the unit cell, the thickness t_d of the dielectric layer and the thickness t_m of the metallic layer. The width of the i^{th} layer, w_i, is directly related to the absorbed frequency by half of its wavelength in the dielectric medium and is calculated by using (2):

$$w_i = \frac{\lambda_i}{2}\frac{1}{\sqrt{\mu_r \varepsilon_r}} \qquad with\ i=1,2,\ldots N \quad (2)$$

with ε_r and μ_r as the real part of the permittivity and the real part of the permeability of the insulator layer respectively, and N as the number of pairs of layers. For the period p, 1 mm is added for each side of the geometry, to the biggest width w. The thickness of the dielectric layers, t_d, is fundamental for the absorption level but no simple closed form was found in the literature [33]. In our model, the dielectric thickness is optimized by considering the printing constraints and by imposing the same thickness to all the dielectric layers. With the value of 0.3 mm, almost unitary absorptivity is reached for 8.5-17.8 GHz. The absorption level was found to be not dependent on the thickness of the conductive layers, therefore, 0.3 mm has been chosen due to the printing restrictions. All the layers, both dielectric and metallic, have the same thickness of 0.3 mm for an overall dimension of 6.3 mm considering the ground plane. The period of the unit cell size is 9.5 mm, the bottom and top layers measure 7.5 mm and 4.2 mm, respectively.

The design and the simulations have been performed using CST Microwave Studio 2018, with two-dimension periodic boundary condition and Floquet modes used as excitation port.

III. FDM Fabrication and X-Ray Analysis

For the fabrication of our prototype, the FDM technique is exploited by using commercial filaments available on the market. For the dielectric layers, the filament Preperm Dk4 [34] is used. Differently from [30], where the measurements of the permittivity was performed with a rectangular cavity directly on the filament, in this paper the transmission method using a coaxial line [35] has been used to characterize a printed sample. A permittivity value of 4.6 was obtained on a 2mm-thickness printed torus over the frequency band of 100 MHz - 18 GHz. For the conductive layers, the filament Electrifi [36] with σ=17000 S/m measured with a 4-points measurement method [37] is employed. The overall dimensions of the structure are 250 mm x 250 mm comprising of 26 x 26 pyramidal elements and a total thickness of 7.8 mm, with 6.3 mm for the printed structure and 1.5 mm for the support layer below the ground plane, Fig. 2(a).

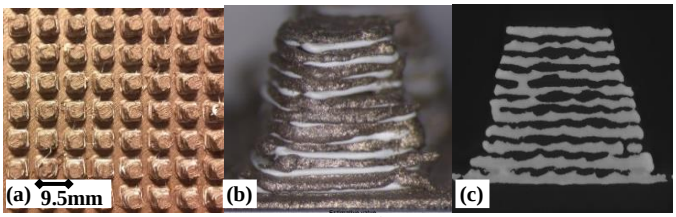

Fig. 2: Fabricated prototype: (a) One area of the complete prototype, top view. Single pyramidal structure, (b) side view, (c) transverse side view using the X-ray analysis.

In Fig. 2(b), a pyramid constituting the dielectric material in white layers and the conductive filament in brown layers is presented. Some imperfections, which can be imputed to the fabrication process, have been analysed with the 3D X-ray CT (Computed Tomography) [38]. The image of one transverse section of the side view of a single pyramid is reported in Fig. 2(c), with the white colour corresponding to the conductive layers. These imperfections, linked to the geometries of the cavities (square shape and layers' thickness), can be explained by the degradation in precision of the FDM technique when using different materials with different glass temperatures. Since Electrifi is a PLA-based filament and Preperm DK4 is an ABS-based filament, there is 40°C of difference in their glass temperatures, leading to some difficulties in printing and less accurate resolution. In contrast with these imperfections, a very good agreement is found for the widths of the layers between the X-ray analysis, based on the average values of all the observed pyramids, and the designed ones with a maximum discrepancy about 5%. Therefore, all the frequency peaks are ensured to be equally spread over the desired absorbed frequency band, resulting in a good performance of the absorber with almost unitary absorption level as presented in the next section.

IV. RF Characterization

The measurements of our sample are conducted both in anechoic chamber (AC) and in non-anechoic chamber (NAC). A free space bi-static setup is assembled in NAC with two Satimo QR2000 antennas which operate at 2-18 GHz and placed at 125cm apart from the sample. Classical foam absorbers loaded with carbon particles are placed between the

two antennas and behind the structure under analysis to eliminate the interferences.

The reflection coefficient is calculated by using (3) [39]:

$$S_{11}(f) = \Gamma^{ABSORBER} = \frac{S_{21}^{total} - S_{21}^{env}}{S_{21}^{env} - S_{21}^{met}} \quad (3)$$

where S_{21} corresponds to the transmission coefficient from antenna 1 to antenna 2, *total* is the measurement performed with the absorber, *env* is the measurement without any sample and *met* is the measurement with a metal plate of 250 mm x 250 mm used as reference. Once S_{11} is obtained, the absorptivity is computed using (1).

In order to evaluate the quality of a broadband absorber, the fractional bandwidth (FB) is used as the figure of merit:

$$FB = \frac{f_{max} - f_{min}}{f_c} = 2\frac{f_{max} - f_{min}}{f_{max} + f_{min}} \quad (4)$$

where f_{min} and f_{max} are the extreme frequencies of the band, in which an absorption coefficient of more than 0.90 is obtained, and f_c the centre frequency.

The measurements performed under normal incidence and in different azimuthal angles φ, rotation angles of the absorber relative to its normal axis, are presented in section A while the behaviours under oblique incidences θ (incidence angle of the incoming wave) are presented in section B. The illustration of θ and φ angles is shown in the insert of Fig. 3 for the horizontal polarization. The green plane corresponds to the incidence plane while the grey plane corresponds to the absorber plane. For section A, the measurements are performed in both AC and NAC, whereas for section B, the measurements are available only for the NAC.

A. Characterization in normal incidence

In bi-static setup, when the two antennas are far enough from the sample and are very close to each other, the measurement can be considered as in normal incidence. In Fig. 3, for φ=0°, an absorption level greater than 0.95 is observed in a wide frequency range from 8.2 GHz to 17.2 GHz, with FB of 0.71 in NAC. The same amount of absorptivity is detected for 8.1-17.8 GHz, with FB of 0.74 in AC. The difference in the NAC measurement result compared to our previous work [30] can be explained by various improvements of the setup environment to increase the measurement dynamic and reduce the interferences. This updated result was validated with a good correlation with the measurements in the anechoic chamber and with the simulation.

The measurements for different 90°-rotations of φ angles are performed in the AC but they are not presented in the paper. Similar behaviours are observed for all the configurations (φ=0°, φ=±90°, φ=180°) thanks to the square symmetry of the geometry with slight differences for the high frequencies at which the risk that some layers are melted or mixed together, therefore ruining the resonance of the cavities, is possible.

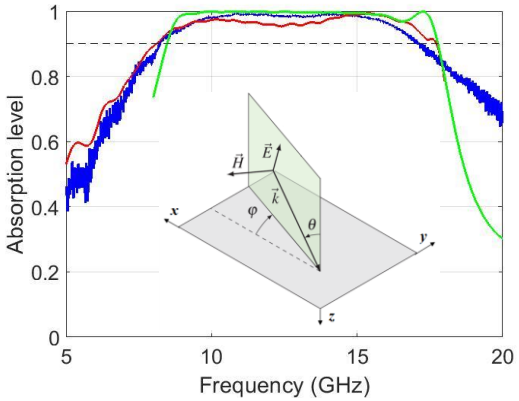

Fig. 3: Comparison between the simulation (green), and the measurements in anechoic chamber (red) and in non-anechoic chamber (blue) for φ = θ = 0°. The definition of φ (azimuth) and θ (elevation incidence) angles are shown in the insert for the horizontal polarization (H-pol.) with the plane of incidence in green and the plane of the structure under test in grey. When **E** and **H** are inverted, vertical polarization (V-pol.) is considered.

B. Characterization in oblique incidences

For the characterization in different θ angles, the measurements are performed only in NAC for different φ angles (0°, ±15°, ±30°, ±45°, ±90°, ±180°). Two cases, the best and the worst performances of the absorber, corresponding to φ=0° and φ=30° respectively, are presented. For the first case, the measurements are compared to the simulations. For the second case, only the characterization is presented. Because of the periodicity of the structure, to ensure no reflection in any diffracted angles, the reflection coefficient was measured by fixing one antenna and manually moving the other one along θ angles. The absorption of all the energy was guaranteed since no significant reflection of energy was registered.

The absorption mechanism, in oblique incidence, is related to the resonance of the cavities. When the absorber is impinged by an electromagnetic wave, for normal incidence, only the fundamental mode and its odd harmonic modes are excited in each cavity [40]. When the absorber is impinged by a wave with oblique incidence, higher order modes, compared to the fundamental one, can be excited. In Fig. 4, the increased absorptivity of the highest frequencies for high oblique incidences can be explained thanks to these modes excited inside the bottom cavities of each hyperbolic structure, both for vertical polarization (V-pol.) and horizontal polarization (H-pol.).

a) Characterization in oblique incidences at φ=0°

A good agreement between simulations and measurements is obtained as depicted in Fig. 4. For the V-pol., in normal incidence, an absorptivity higher than 0.95 is measured for 8.2-17.2 GHz (FB=0.71) and both the bandwidth and the absorption level remain constant up to 10°. From 10° to 40° the effective widths of the cavities, seen from the incident wave, are smaller than in the previous case, where the resonant condition of $\lambda_g/2$ is satisfied (with $\lambda_g = \lambda_i/\sqrt{\mu_r \varepsilon_r}$), and a shift toward the higher frequencies is observed. An absorptivity bigger than 0.90 is calculated for 9.0-20.0 GHz (and more), thanks to the higher order modes excited in the lower part of the structure, up to θ=50°. Instead, for the H-

pol., in normal incidence, an absorption level higher than 0.90 is obtained over 8.2-17.3 GHz (FB=0.71). When increasing the incident angles, the 0.9-absorption bandwidth constantly decreases. At θ=50°, an FB of 0.31 (9.7-13.3 GHz) is observed.

The difference in absorption level between the two polarizations is due to the different excitations of the current flux density. This is linked to the magnitude of the parallel component of the electric field **E** to the absorber plane, corresponding to the xy plane in the insert of Fig. 3**.** Referring to this insert, for the H-pol., **E** can be decomposed into parallel component $\mathbf{E_x}$ and orthogonal component $\mathbf{E_z}$; the magnitude of the parallel component $\mathbf{E_x}$ decreases with θ and a lower current flux density is excited, leading to an absorptivity degradation in H-pol. when increasing θ angle. For the V-pol., the **E** field is always parallel to the xy-plane and its magnitude does not change with θ leading to a better absorptivity compared to H-pol..

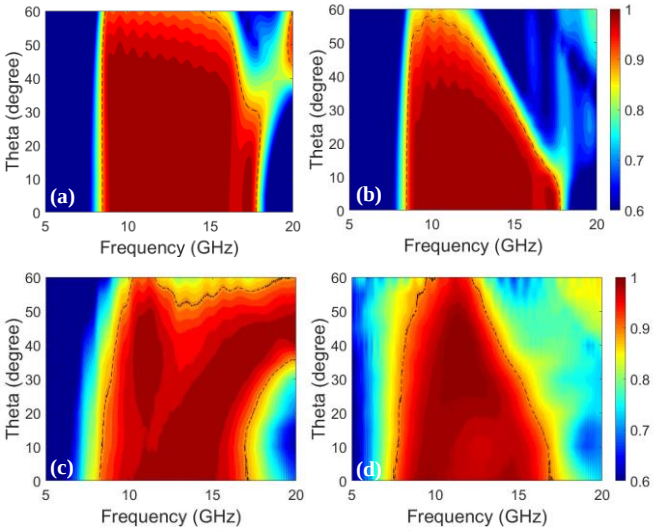

Fig. 4: Absorption level for φ=0°: simulations for (a) vertical polarization and (b) horizontal polarization, and measurements in non-anechoic chamber for (c) vertical polarization and (d) horizontal polarization. The dashed line in black corresponds to an absorptivity of 0.90.

b) Characterization in oblique incidences at φ=30°

A similar behaviour to the one in the previous case can be seen here. For the V-pol., an absorption level above 0.90 for the band 8.0-16.3 GHz (FB=0.68) is obtained from normal incidence and maintained up to 25°. A smaller absorbed bandwidth is measured due to the smaller effective width of the cavities seen from the incoming wave. Compared to the case at φ=0°, the absorptivity of 0.90 does not cover all the wide frequency band and a slightly lower absorptivity of 0.85 is observed in a sub-range from 12 GHz to 14 GHz from 25° to 50°. For the H-pol, under normal incidence, absorptivity above 0.90 for the frequency range of 8.3-16.6 GHz (FB=0.67) is calculated and it decreases up to 50° for the band 9.3-13.8 GHz (FB=0.39). The degraded performances, in respect to the first case, could be explained by the symmetry of the structure. Thanks to its square shape, the absorber responds well to rotations of 90° while at a rotation of 30°, the symmetry is no longer respected. While for the high frequencies this problem is compensated with the higher order modes of the cavities on the bottom, for the middle frequency range there are no resonances of higher order modes resulting in a slight absorptivity drop in the central frequency band. Hyperbolic metamaterial with circular shape could be used to avoid symmetry problems linked to φ angles.

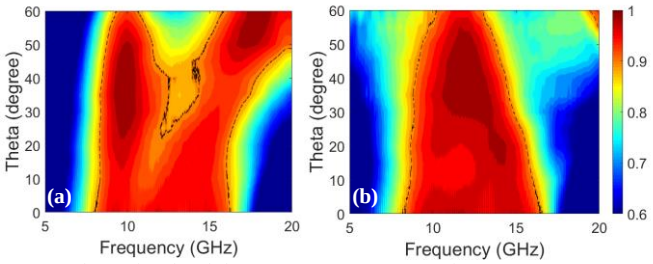

Fig. 5: Absorption level for φ=30°: measurements in non-anechoic chamber for (a) vertical and (b) horizontal polarization. The dashed line in black corresponds to an absorptivity of 0.90.

V. Conclusion

A fully 3D-printed hyperbolic metamaterial absorber, working in the X and K_u bands with an absorption level above 0.9 under normal incidence, was presented in this paper. The dissipated power increased with the resistive losses introduced by the conductive filaments allows a flat absorptivity bandwidth. Thanks to the different degrees of freedom in modelling offered by the Fused Deposition Modeling technique, the design of each resonant cavity has been engineered to have equally spaced frequency peaks spread over the targeted absorption band, that permit a unitary absorption level. The dimensional analysis of the manufactured absorber was conducted with the X-ray to confirm the correct width of each cavity. Two cases, corresponding to the best and the worst performances of the absorber, were presented. For both cases, the best absorption was obtained for the V-pol.. The differences between the two cases were found linked to the effective geometries seen from the incident wave, which impact the total bandwidth for both polarizations. Indeed, for the V-pol., an absorption level above 0.90 is observed over the FB of 0.71 from normal incidence up to 50° in the first case and above 0.85 over the FB of 0.68 from normal incidence up to 50° in the second case. For the H-pol, a similar performance was found as for the V-pol. under normal incidence, and at θ=50° and φ=30° only a FB of 0.39 is covered by an absorption level above 0.90. Thanks to the presented results and the fast developing of additive manufacturing, we consider this technology, exploiting both arbitrary geometries, which could be a conical shape to improve the performances under different φ and θ angles, and ad hoc materials with tailored electromagnetic properties, as a possible future leader in radar absorbing material.

Acknowledgement

This work has been partly funded by the French MOD. The authors would like to thank Carole Jégou and Philippe Pouliguen for helpful technical discussions. A special thanks to Isabelle Le Roy Naneix and Thierry Arreteau for the possibility to measure the absorber in the anechoic chamber.

REFERENCES

[1] W.W. Salisbury, "Absorbent Body for Electromagnetic Waves," U.S. patent 2 599 944, June, 10, 1952.

[2] M. Barbuto, A. Monti, D. Ramaccia, F. Bilotti, and A. Toscano, "Design and realization of MTM-inspired absorbers using graphite resistive sheets," *AIP Conference Proceedings*, vo. 1648, no. 1, pp. 570012, Apr., 1, 2015. DOI: https://doi.org/10.1063/1.4912798.

[3] L. J. Du Toit, "The design of Jauman absorbers," *IEEE Antennas and Propagation Magazine*, vol. 36, no. 6, pp. 17-25, Dec. 1994. DOI: 10.1109/74.370526.

[4] E.F. Knott, J.F. Schaeffer and M.T. Tuley, "Radar Absorbing Materials," in Radar Cross Section, 2nd ed., Raleigh, NC, USA: SciTech Publishing, 2004, ch 8, sec 8.4, pp. 313-327.

[5] K. N. Rozanov, "Ultimate thickness to bandwidth ratio of radar absorbers," *IEEE Transactions on Antennas and Propagation*, vol. 48, no. 8, pp. 1230-1234, Aug. 2000. DOI: 10.1109/8.884491.

[6] N. Engheta, "Thin absorbing screens using metamaterial surfaces," *IEEE Antennas and Propagation Society International Symposium (IEEE Cat. No.02CH37313)*, San Antonio, TX, USA, 2002, pp. 392-395 vol.2. DOI: 10.1109/APS.2002.1016106.

[7] F. Bilotti, L. Nucci, and L. Vegni, "An SRR based microwave absorber," *Wiley Periodicals Inc., Microwave and Opt. Technol. Lett.*, Vol. 48, no. 11, pp 2171-2175, Nov., 2006, DOI 10.1002/mop.21891.

[8] F. Bilotti, A. Toscano, K. B. Alici, E. Ozbay and L. Vegni, "Design of Miniaturized Narrowband Absorbers Based on Resonant-Magnetic Inclusions," *IEEE Transactions on Electromagnetic Compatibility*, vol. 53, no. 1, pp. 63-72, Feb. 2011. DOI: 10.1109/TEMC.2010.2051229.

[9] C. M. Watts, X. Liu, and W. J. Padilla, "Metamaterial electromagnetic wave absorbers," *Adv. Mater*., vo. 24, no. 23, June, 24, 2012, pp. OP98-OP120. DOI: 10.1002/adma.201200674.

[10] Y. Ra'Di, C. R. Simovski, and S. A. Tretyakov, "Thin Perfect Absorbers for Electromagnetic Waves Theory, Design, and Realizations," *Phys. Rev. Applied*, vo. 3, no. 3, pp. 037001-1-37, Mar., 17, 2015. DOI:10.1103/PhysRevApplied.3.03700.

[11] A. Kazemzadeh, "Nonmagnetic Ultrawideband Absorber With Optimal Thickness," *IEEE Transactions on Antennas and Propagation*, vol. 59, no. 1, pp. 135-140, Jan. 2011. DOI: 10.1109/TAP.2010.2090481.

[12] O. Luukkonen, F. Costa, C. R. Simovski, A. Monorchio and S. A. Tretyakov, "A Thin Electromagnetic Absorber for Wide Incidence Angles and Both Polarizations," *IEEE Transactions on Antennas and Propagation*, vol. 57, no. 10, pp. 3119-3125, Oct. 2009. DOI: 10.1109/TAP.2009.2028601.

[13] F. Costa, A. Monorchio and G. Manara, "Analysis and Design of Ultra Thin Electromagnetic Absorbers Comprising Resistively Loaded High Impedance Surfaces," *IEEE Transactions on Antennas and Propagation*, vol. 58, no. 5, pp. 1551-1558, May 2010. DOI: 10.1109/TAP.2010.2044329.

[14] Lei Lei, Shun Li, Haixuan Huang, Keyu Tao, and Ping Xu, "Ultra-broadband absorber from visible to near-infrared using plasmonic metamaterial," *Opt. Express*, vo. 26, no.5, pp. 5686-5693, Mar., 5, 2018. DOI: https://doi.org/10.1364/OE.26.005686.

[15] N. I. Landy, S. Sajuyigbe, J. J. Mock, D. R. Smith, and W. J. Padilla, "Perfect Metamaterial Absorber," *Phys. Rev. Lett.*, vo. 100, no. 20, pp. 207402-1-4, May, 18, 2008, DOI: 10.1103/PhysRevLett.100.207402.

[16] Hou-Tong Chen, "Interference theory of metamaterial perfect absorbers," *Opt. Express*, vo. 20, no. 7, pp. 7165-7172, Mar., 26, 2012. DOI: https://doi.org/10.1364/OE.20.007165.

[17] A. Poddubny, I. Iorsh, P. Belov and Yuri Kivshar, "Hyperbolic Metamaterials," *Nature photonics*, vo. 7, pp. 948–957, Nov., 28, 2013. DOI:https://doi.org/10.1038/nphoton.2013.243.

[18] Vora, A., Gwamuri, J., Pala, N. et al. "Exchanging Ohmic Losses in Metamaterial Absorbers with Useful Optical Absorption for Photovoltaics," *Sci. Rep.*, vo. 4, pp. 4901, May, 9, 2015. DOI: https://doi.org/10.1038/srep04901.

[19] N. Fernez et al., "Radiative Quality Factor in Thin Resonant Metamaterial Absorbers," *IEEE Transactions on Microwave Theory and Techniques*, vol. 66, no. 4, pp. 1764-1772, April 2018. DOI: 10.1109/TMTT.2017.2784808.

[20] Y. Cui, K. H. Fung, J. Xu, H. Ma, Y. Jin, S. He, and N. X. Fang, "Ultrabroadband Light Absorption by a Sawtooth Anisotropic Metamaterial Slab," *Nano Lett*., vo. 12, no. 3, pp. 1443-1447, Feb., 6, 2012. DOI: 10.1021/nl204118h.

[21] F. Ding, Y. Cui, X. Ge, F. Zhang, Y. Jin, and S. He, "Ultra-broadband microwave metamaterial absorber," *Appl. Phys. Lett.*, vo. 100, no. 10, pp. 103506, Mar., 09, 2012. DOI: https://doi.org/10.1063/1.3692178.

[22] C. Long, S. Yin, W. Wang, W.Li, J. Zhu and J. Guan, "Broadening the absorption bandwidth of metamaterial absorbers by transverse magnetic harmonics of 210 mode," *Sci. Rep*., vo. 6, pp. 21431, Feb., 18, 2016. DOI: https://doi.org/10.1038/srep21431.

[23] J. Zhu, Z. Ma, W. Sun, F. Ding, Q. He, L. Zhou and Y. Ma, "Ultra-broadband terahertz metamaterial absorber," *Appl. Phys. Lett.*, vo. 105, no. 2, pp. 021102, Jul., 14, 2014. DOI: 10.1063/1.4890521.

[24] F. M. Espiau and G. P. Le Sage, "3D Printed Radio Frequency Absorber", U.S. patent 15 064 451, Sep., 15, 2016.

[25] R. Kronberger and P. Soboll, "New 3D printed microwave metamaterial absorbers with conductive printing materials," at *46th European Microwave Conference (EuMC)*, London, 2016, pp. 596-599. DOI: 10.1109/EuMC.2016.7824413.

[26] D. Zhou, X. Huang and Z. Du, "Analysis and Design of Multilayered Broadband Radar Absorbing Metamaterial Using the 3-D Printing Technology-Based Method," *IEEE Antennas and Wireless Propagation Letters*, vol. 16, pp. 133-136, 2017. DOI: 10.1109/LAWP.2016.2560904.

[27] W. Jiang, L. Yan, H. Ma1, Y. Fan, J. Wang, M. Feng, and S. Qu, "Electromagnetic wave absorption and compressive behavior of a three-dimensional metamaterial absorber based on 3D printed honeycomb," *Sci. Rep.*, vo. 8, pp. 4817, Mar., 19, 2018. DOI: https://doi.org/10.1038/s41598-018-23286-6.

[28] J. Ren, and J. Y. Yin, "3D-Printed Low-Cost Dielectric-Resonator-Based Ultra-Broadband Microwave Absorber Using Carbon-Loaded Acrylonitrile Butadiene Styrene Polymer," *Materials*, vo. 11, no. 7, pp. 1249, July, 20, 2018. DOI: https://doi.org/10.3390/ma11071249.

[29] P. J. Bradley, M. O. M. Torrico, C. Brennan, and Y. Hao, "Printable all-dielectric water-based absorber," *Sci. Rep.*, vo. 8, pp. 14490, Sep., 27, 2018. DOI: https://doi.org/10.1038/s41598-018-32395-1.

[30] X. Lleshi, R. Grelot, T. Q. Van Hoang, B. Loiseaux and D. Lippens, "Wideband Metal-Dielectric Multilayer Microwave Absorber based on a Single Step FDM Process," *2019 49th European Microwave Conference (EuMC)*, Paris, France, 2019, pp. 678-681. DOI: 10.23919/EuMC.2019.8910777.

[31] J. Ren, and J.Y. Yin, "Cylindrical water resonator based ultra-broadband microwave absorber," *Opt. Mater. Express*, vol. 8, no.8, pp. 2060-2071, Aug., 1, 2018. DOI: https://doi.org/10.1364/OME.8.002060.

[32] T. Liu, Y. Xu, D. Zheng, L. Zhou, X. Li and L. Liu, "Fabrication and absorbing property of the tower-like absorber based on 3D printing process," *Physica B: Condensed Matter*, vo. 553, pp. 88-95, Jan., 19, 2019. DOI: https://doi.org/10.1016/j.physb.2018.10.038.

[33] K. Y. Bliokh, Y. P. Bliokh, V. Freilikher, S. Savel'ev, and F. Nori, "Colloquium: Unusual resonators: Plasmonics, metamaterials, and random media", *Rev. Mod. Phys.*, vo. 80, no. 4, pp. 1201-1213, Oct., 1, 2008. DOI: https://link.aps.org/doi/10.1103/RevModPhys.80.1201.

[34] Preperm, https://www.preperm.com/products/stock-shapes/#filaments

[35] M. A. Stuchly and S. S. Stuchly, "Coaxial Line Reflection Methods for Measuring Dielectric Properties of Biological Substances at Radio and Microwave Frequencies-A Review," *IEEE Transactions on Instrumentation and Measurement*, vol. 29, no. 3, pp. 176-183, Sept. 1980. DOI: 10.1109/TIM.1980.4314902.

[36] Electrifi, https://www.multi3dllc.com/about-electrifi/

[37] F. M. Smits, "Measurement of sheet resistivities with the four-point probe," *The Bell System Technical Journal*, vol. 37, no. 3, pp. 711-718, May 1958. DOI: 10.1002/j.1538-7305.1958.tb03883.x.

[38] J. Hsieh, *Computed Tomography: Principles, Design, Artifacts, and Recent Advances*, 2nd ed., Bellingham, WA, USA, Spie Press Book, 2009.

[39] L. Pometcu, A. Sharaiha, R. Benzerga, R. D. Tamas and P. Pouliguen, "Method for material characterization in a non-anechoic environment," *Appl. Phys. Lett*., vol. 108, no. 16, April, 22, 2016. DOI: https://doi.org/10.1063/1.4947100.

[40] X. Y. Peng, B. Wang, S. Lai, D. H. Zhang and J. H. Teng, "Ultrathin multi-band planar metamaterial absorber based on standing wave resonances," Optics Express, vol. 20, no. 25, Dec. 2012. DOI: https://doi.org/10.1364/OE.20.027756.